

# Pairing from repulsion in a two-dimensional Fermi gas with soft-core interactions

Ahmet Keles,<sup>1</sup> Xiaopeng Li,<sup>2,3,4</sup> and Erhai Zhao<sup>5</sup>

<sup>1</sup>*Department of Physics, Middle East Technical University, Ankara 06800, Turkey*

<sup>2</sup>*State Key Laboratory of Surface Physics, Key Laboratory of Micro and Nano Photonic Structures (MOE), and Department of Physics, Fudan University, Shanghai 200433, China*

<sup>3</sup>*Shanghai Qi Zhi Institute, AI Tower, Xuhui District, Shanghai 200232, China*

<sup>4</sup>*Shanghai Research Center for Quantum Sciences, Shanghai 201315, China*

<sup>5</sup>*Department of Physics and Astronomy, George Mason University, Fairfax, Virginia 22030, USA*

We investigate a model many-body system of spinless Fermi gas in two dimensions, where the bare two-body interaction is repulsive and takes the form of a soft-core disk potential. We obtain the zero temperature phase diagram of this model by numerical functional renormalization group (FRG), which retains the effective interaction vertices in all channels to provide a detailed picture of how Cooper pairing emerges under the renormalization flow. The repulsion drives the system to a series of superfluid states with higher angular momentum pairing, for example in the  $f$ - and  $h$ -wave channels instead of the  $p$ -wave channel. This is in sharp contrast to the original Kohn-Luttinger mechanism where pairing of very large angular momenta and exponentially small transition temperature was predicted. We trace the stabilization and enhancement of  $f$ - and  $h$ -wave pairing back to the momentum dependence of the bare interaction. A perturbative calculation is carried out to show that while the second order Kohn-Luttinger diagrams provide a qualitative understanding of the onsets of the various superfluid phases, they are unable to accurately capture the phase boundaries predicted by FRG. Our findings suggest that tuning the shape of the interaction potential offers a promising route to achieve stronger “pairing glue” and to realize nontrivial superfluid phases in repulsive Fermi gases beyond the scope of the original Kohn-Luttinger analysis.

## I. INTRODUCTION

It remains a long-standing goal to realize non- $s$ -wave superfluids in ultracold Fermi gases. For example, the conventional wisdom to realize the  $p_x + ip_y$  state in spin-polarized (single-species) Fermi gases is to bring it close to a  $p$ -wave Feshbach resonance where the  $p$ -wave interaction between two fermionic atoms becomes attractive [1–4]. Unfortunately, this effort has been hampered by severe three-body losses near the resonance. Despite the recent success in improving the gas lifetime in one- and three-dimensional optical lattices [5–8], it remains a challenge to suppress the atom loss. Here in this paper, we explore an alternative route that does not require  $p$ - or higher-wave resonances. In particular, we address the following questions: Is there room for superfluidity in polarized Fermi gases if the bare interaction is *purely repulsive*? If so, in which parameter regimes is the superfluid transition temperature  $T_c$  enhanced and thus more accessible by experiments?

Central to these questions is the issue of “pairing glue” in a repulsive Fermi liquid. The term “pairing glue” is often used in the literature on quantum materials, and it refers to the microscopic mechanism that binds the fermions into Cooper pairs [9, 10]. It is well known that in most conventional  $s$ -wave superconductors, phonons act as the glue [11]. On the other hand, while there is no consensus yet, spin fluctuations are likely responsible for the  $d$ -wave pairs observed in cuprate superconductors, or the the putative  $d$ -wave superfluid phase of the repulsive Fermi-Hubbard model (for a review see for instance [12, 13]). For continuum gases of spinless fermions, however, neither lattice vibration nor spin fluctuation is

present, so only density fluctuation can step in to make the glue. Since the system cannot remain a Fermi liquid down to zero temperature, it is long believed that many-body effects will turn the repulsive bare interaction into attractive effective interaction in certain pairing channels. In other words, the force between two fermions may flip sign under renormalization [14].

A well-known example is the Kohn-Luttinger (KL) mechanism discovered by W. Kohn and J. M. Luttinger back in 1965 [15, 16]. They showed that for spin 1/2 fermions in three dimensions (3D) with weak short-range repulsive interactions, the effective interaction  $\Gamma_\ell$  in the  $\ell$ -th angular momentum channel always turns attractive for sufficiently high partial waves, e.g. some odd  $\ell \gg 1$ . This means that a repulsive Fermi liquid is always unstable against pairing (there may be other competing instabilities as well), albeit the corresponding  $T_c \propto e^{-\alpha\ell^4}$ , with  $\alpha$  some constant, is exponentially small [15]. Fay and Layzer generalized the KL analysis for large  $\ell$  to include small  $\ell$ . In the dilute limit, regardless the strength of the interactions, they found the dominant instability is toward a  $p$ -wave superfluid with  $\ell = 1$  [17]. Kagan and Chubukov reached the same conclusion and computed the  $T_c$  [18]. The KL effect in two dimensions (2D) requires a more delicate analysis beyond second order perturbation theory, but as shown by Chubukov [19], the dominant pairing instability remains in the  $p$ -wave channel. We stress that all these results were obtained for spin-1/2 fermions where the bare interaction is replaced by a pseudopotential that can be parametrized by the  $s$ -wave scattering length  $a$  [15].

The main goal of this paper is to understand how repulsion drives pairing in spinless Fermi gas in two dimen-

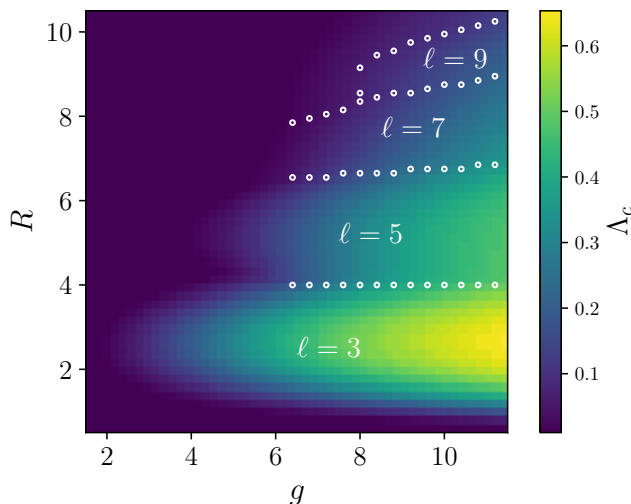


FIG. 1. The FRG phase diagram of a repulsive Fermi gas in 2D: the superfluid phases resemble four fingers of a hand (with the thumb  $\ell = 1$  missing). The Cooper pair angular momentum is  $\ell = 3$  ( $f$ -wave), 5 ( $h$ -wave), 7 and 9 respectively. The model and the dimensionless interaction strength  $g$  are defined in Section II, and the interaction range  $R$  is measured in  $1/k_F$ , the inverse Fermi momentum. The empty circles mark the phase boundaries, and the “critical scale”  $\Delta_c$  in false color gives a rough estimate of the superfluid  $T_c$ .

sions from the modern perspective of functional renormalization group (FRG). We focus on a simple model of bare interaction in the form of the disk potential Eq. (1) which is often referred to as the square (or step function) potential in quantum mechanics textbooks. In order to go beyond the aforementioned KL analysis, we treat the many-body problem using FRG which goes beyond leading order perturbation theory and retains the interaction vertices in all (e.g. pairing, density wave, and Pomeranchuk) channels. We solve the FRG flow equation numerically to obtain the full phase diagram and compare the transition temperature in different parameter regions. The main results are summarized in Fig. 1. We observe that, surprisingly, the behaviors of this system differ significantly from the classical KL results outlined in the preceding paragraph. For instance,  $f$ -wave or  $h$ -wave (instead of  $p$ -wave) superfluid states are stabilized, and their transition temperatures are not exponentially small.

To gain further understanding of the numerical FRG result, we also carry out a perturbative calculation which becomes accurate in the dilute (low density) limit. We show that evaluation of the so-called KL diagrams for our model yields results in qualitative agreement with FRG. The perturbative calculation enables us to see how and when the effective interaction  $\Gamma_\ell$  turns negative, and why it differs significantly from the well-known KL physics in spin-1/2 systems. The calculation also illustrates the limitations of perturbation theory. For example, the predicted phase boundaries (see Fig. 10) deviate significantly from the FRG phase diagram (Fig. 1) which is

much more accurate because it includes many-body processes well beyond the KL diagrams.

The bare potential Eq. (1), as a simple model to elucidate the intriguing many-body physics, may not be easily realized in experiments. Our model choice however is not arbitrary and in fact inspired by the interaction potential in Rydberg-dressed Fermi gases which recently became available in experiments [20]. In Ref. [21], three of us discovered that an  $f$ -wave superfluid naturally emerges in these systems even when the bare Rydberg-dressed interaction is repulsive. The disk potential here retains the soft-core part of Rydberg-dressed potential but discards its long-range tail. By comparing the phase diagrams of the two models, one makes an important observation: it is the repulsive core, rather than the long-range tail, that is crucial to  $f$ -wave pairing. The current model also features a much richer phase diagram. The perturbative analysis (Section IV) and its comparison against FRG are also new results beyond the scope of Ref. [21].

Our results for model Eq. (1) makes it clear that *the shape of the bare interaction matters* to enhancing the pairing glue in repulsive Fermi gases. A nice feature of the disk-potential  $V(r)$  is that its Fourier transform  $v(q)$  develops oscillations and becomes attractive for certain range of momenta, see Eq. (3). This is in contrast to previous works on spin-1/2 Fermi gases, where  $v(q)$  is usually assumed to be a constant  $u$ . Under renormalization, these attractive segments of  $v(q)$  feed to the flow of the effective interaction  $\Gamma_\ell$  toward negative values, eventually leading to a slew of superfluid phases with  $\ell = 3, 5, 7, 9, \dots$  in Fig. 1 (this feature is absent in Ref. [21]). In the original KL picture [15], the effective interaction between two fermions acquires a long-range oscillatory part because of the sharp Fermi surface, which is related to the Friedel oscillations in real space. In our case, we have not only a sharp Fermi surface (a step function in momentum space), but also a sharp two-body interaction potential (a step function in real space). This *double whammy* also partly explains why the  $T_c$  of these superfluid phases is not exponentially small as in the original KL analysis. To our knowledge, the importance of the interaction shape has not received a lot of attention in the literature. We hope the model study presented here can stimulate new ideas to engineer stronger pairing glues by shaping the bare interactions. Our results suggest that this is a promising route to observe higher angular momentum pairing in repulsive Fermi gases.

## II. MODEL AND BARE INTERACTION

Our model is a spin-polarized (spinless) Fermi gas in 2D with the short-range interaction potential

$$V(r) = V_0 \theta(R - r). \quad (1)$$

Here  $r$  is the distance between two fermions,  $\theta(x)$  is the Heaviside step function,  $R$  is the radius of the disk, and  $V_0 > 0$  is the interaction strength. In the limit of large

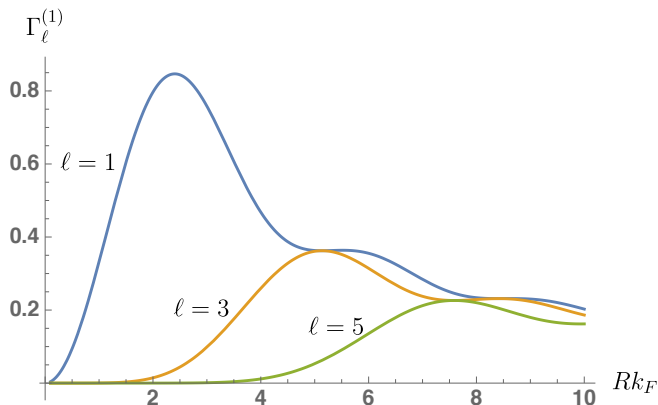


FIG. 2. The bare interaction  $\Gamma_\ell^{(1)}$  in angular momentum channel  $\ell = 1$  (blue), 3 (orange), and 5 (green), all being repulsive.  $\Gamma_\ell^{(1)}$  is defined in Eq. (5) for two fermions on the Fermi surface and measured in unit of  $(2\pi R^2 V_0)$ .

$V_0$ ,  $V(r)$  gives the hard-disk potential (not hard-sphere because we are in 2D). For this reason, we shall call Eq. (1) the soft-core disk potential. Let  $k_F$  be the Fermi momentum,  $m$  the mass of the fermion, then the density of state is  $\mathcal{N} = m/2\pi\hbar^2$  (we will set  $\hbar = 1$  hereafter). We define dimensionless parameter

$$g = (2\pi R^2 V_0) \mathcal{N} \quad (2)$$

which measures the strength of interaction. Another independent dimensionless parameter is  $k_F R$ , which measures the range of the interaction in units of  $1/k_F$ . In Ref. [21], similar parameters were defined for the Rydberg-dressed Fermi gases.

Let us look at the bare interaction in more detail. The Fourier transform of  $V(r)$  is given by the Bessel function

$$v(q) = 2\pi V_0 R^2 \frac{J_1(qR)}{qR} \quad (3)$$

with  $q = |\mathbf{q}|$ , and  $\mathbf{q}$  is the momentum. The function  $v(q)$  is a damped oscillation and turns negative repeatedly. For example, its first negative minimum is at  $x = qR = 5.136$ , where  $J_1(x)/x = -0.06614$ . Again, it is useful to compare it to the Meijer G-function discussed in Ref. 21 which only has one negative minimum. For pairing, the relevant bare interaction is between two fermions on the Fermi surface at momentum  $\mathbf{p}_F$  and  $\mathbf{p}'_F$  respectively, i.e.  $v(|\mathbf{p}_F - \mathbf{p}'_F|)$ . Let  $\phi$  be the angle between  $\mathbf{p}_F$  and  $\mathbf{p}'_F$ , the bare interaction can be written as

$$\Gamma_\ell^{(1)}(\phi) = v(2k_F |\sin \frac{\phi}{2}|). \quad (4)$$

Here the superscript of  $\Gamma^{(1)}$  emphasizes that this is the leading order (to order  $V_0$ ) contribution from the perspective of perturbation theory. We can decompose  $\Gamma^{(1)}(\phi)$  into angular momentum channels by defining

$$\Gamma_\ell^{(1)} = \int d\phi \Gamma^{(1)}(\phi) \cos(\ell\phi), \quad \ell = 1, 3, 5, \dots \quad (5)$$

Only odd  $\ell$  values are taken, because we are dealing with spinless fermions. The integral in Eq. (5) can be evaluated analytically by exploiting the properties of Bessel functions. The results are plotted in Fig. 2 for  $\ell = 1, 3, 5$ . We observe that  $\Gamma_\ell^{(1)}$  are all positive. This is as expected, for the bare repulsion does not directly lead to Cooper pairing (to order  $V_0$ ). We need many-body effects to induce effective attraction to overcome the bare repulsion.

### III. MAIN RESULTS FROM FRG

We analyze the interacting fermion problem by Functional Renormalization Group (FRG) [22, 23]. Technical details of the FRG approach to 2D continuum Fermi gases can be found in Refs. 21 and 24, and our implementation here follows Ref. 21 closely. For examples of FRG applied to Fermi gases on optical lattices, see Refs. [25–27]. We obtain the zero temperature phase diagram using the following procedure. Starting from an ultraviolet scale  $\Lambda_{UV}$ , where the effective interaction equals to the anti-symmetrized bare interaction, we slowly slide down the momentum scale  $\Lambda \rightarrow \Lambda - \delta\Lambda$  by successively integrating out the higher energy, shorter wavelength fluctuations. The result is a set of coupled flow equations, e.g., for the self-energy  $\Sigma$

$$\partial_\Lambda \Sigma_{1',1} = - \sum_2 S_2 \Gamma_{1',2;1,2}, \quad (6)$$

and for the four-fermion vertex  $\Gamma$

$$\begin{aligned} \partial_\Lambda \Gamma_{1',2';1,2} = \sum_{3,4} (G_3 S_4 + S_3 G_4) & \left[ \frac{1}{2} \Gamma_{1',2';3,4} \Gamma_{3,4;1,2} \right. \\ & \left. - \Gamma_{1',4;1,3} \Gamma_{3,2';4,2} + \Gamma_{2',4;1,3} \Gamma_{3,1';4,2} \right]. \quad (7) \end{aligned}$$

Here 1, 2 ( $1', 2'$ ) label the incoming (outgoing) legs of the effective interaction  $\Gamma$ , and we have used the short-hand notation  $1 \equiv (\omega_1, \mathbf{p}_1)$  to denote the fermion frequency  $\omega$  and momentum  $\mathbf{p}$ . The sum in Eqs. (6)-(7) includes integration over frequency and momentum, e.g.,

$$\sum_3 (\dots) = \int \frac{d\omega_3 d^2 \mathbf{p}_3}{(2\pi)^3} (\dots).$$

Eq. (6) and Eq. (7) can be represented diagrammatically. The first term inside the square bracket in Eq. (7) gives the BCS diagram in the particle-particle channel, while the second (third) term gives the ZS (ZS') diagram in the particle-hole channel. Here ZS stands for zero sound [28]. The term  $(G_3 S_4 + S_3 G_4)$  on the right hand side of Eq. (7) is the analogue of the polarization bubble, but it has a crucial difference as it involves two scale-dependent Green functions defined by

$$G_{\omega,\mathbf{p}} = \frac{\theta(|\xi_{\mathbf{p}}| - \Lambda)}{i\omega - \xi_{\mathbf{p}} - \Sigma_{\omega,\mathbf{p}}}, \quad S_{\omega,\mathbf{p}} = \frac{\delta(|\xi_{\mathbf{p}}| - \Lambda)}{i\omega - \xi_{\mathbf{p}} - \Sigma_{\omega,\mathbf{p}}}, \quad (8)$$

where  $\xi_{\mathbf{p}} = \mathbf{p}^2/2m - E_F$ , with  $E_F$  the Fermi energy. We stress that  $G$ ,  $S$ ,  $\Sigma$  and  $\Gamma$  all depend on the sliding scale

$\Lambda$ , even though we have suppressed the  $\Lambda$ -dependence in our notation for brevity.

The FRG flow equations are formally exact, but in practice they must be truncated and approximated in order for the numerical calculation to become feasible. Higher order contributions have been dropped from Eqs. (6) and (7). We further neglect the frequency dependence of  $\Gamma$  and drop  $\Sigma$ , which is typically not necessary to reveal the leading instabilities. Finally, we project the momenta radially onto the Fermi surface because the angular dependence is most relevant, and accordingly we discretize the Fermi surface evenly into  $N$  patches. Then,  $\Gamma$  is reduced to a three-dimensional array,

$$\Gamma_{1',2';1,2} \rightarrow \Gamma(\mathbf{p}'_{F1}, \mathbf{p}'_{F2}, \mathbf{p}_{F1}) \rightarrow \Gamma_{i,j,k}.$$

Here only three momentum variables are needed thanks to the conservation of the total momentum, and  $i, j, k = 1, 2, \dots, N$  are the patch indices giving the angular position on the circular Fermi surface. We stress that similar truncation and approximation schemes have been extensively employed and benchmarked in the application of FRG to correlated electrons. For a detailed assessment and justification of these steps, the readers may consult the review Ref. [22]. In principle, one can systematically include higher order diagrams and take into account the frequency dependences. These improvements however come with a steep increase in the requirement of computing resources.

Even with these simplifications, the computation remains heavy. For example, for an angular grid with  $N = 128$ ,  $\Gamma$  contains  $N^3$ , roughly 2 million, elements. We call them running couplings, because they undergo non-trivial evolutions as  $\Lambda$  is reduced. Among all the running couplings, the largest absolute value is denoted as

$$\Gamma_{max} = \max|\Gamma_{i,j,k}|.$$

From  $\Gamma$ , we also construct the channel matrix for BCS pairing

$$V_{\text{BCS}}(\mathbf{p}', \mathbf{p}) = \Gamma(\mathbf{p}', -\mathbf{p}', \mathbf{p}). \quad (9)$$

and the channel matrix for charge density wave (CDW) order with wavevector  $\mathbf{q}$

$$V_{\text{CDW}}^{\mathbf{q}}(\mathbf{p}', \mathbf{p}) = \Gamma(\mathbf{p} + \mathbf{q}/2, \mathbf{p}' - \mathbf{q}/2, \mathbf{p} - \mathbf{q}/2). \quad (10)$$

Another example is the Pomeranchuk channel

$$V_{\text{POM}}(\mathbf{p}', \mathbf{p}) = \Gamma(\mathbf{p}, \mathbf{p}', \mathbf{p}), \quad (11)$$

the instability of which points to spontaneous deformation of the Fermi surface. With these approximations, the flow equation (7) is solved numerically by sliding  $\Lambda$  on a logarithmic grid from the ultraviolet (UV) scale  $\Lambda_{UV} = E_F$  down to a very small infrared (IR) scale, e.g.,  $\Lambda_{IR} = 0.01E_F$ . Typically we have hundreds of grid points along the  $\Lambda$  axis, and at each RG step, the most time consuming part is the summation over internal lines,

$\sum_{3,4}$  in Eq. (7). The calculation is checked to ensure the result does not change upon further refining the angular or  $\Lambda$  grids.

To detect possible many-body instabilities of the interacting Fermi gas, we monitor the flow of  $\Gamma$  and look for signs of divergence as  $\Lambda \rightarrow 0$ . For example, a clear signal of divergence is when  $\Gamma_{max}$  quickly exceeds a large threshold such as  $100E_F$  at some ‘‘critical value’’  $\Lambda = \Lambda_c$ . In such cases we record  $\Lambda_c$  and use it as an estimate of the  $T_c$  of the corresponding broken symmetry phase. In other cases (see Fig. 5 below), the flow continues smoothly down to  $\Lambda_{IR}$ , indicating the Fermi liquid is stable down to this temperature scale, within the approximation and numerical precision of our calculation. The channel matrices defined above provide a systematic way to identify the broken symmetry phases. In each channel  $ch \in \{\text{BCS, CDW, POM, ...}\}$  and at each RG step, we diagonalize the channel matrix  $V_{ch}$  and record its most negative eigenvalue  $\Gamma_{min}^{ch}$  (for density waves, we also vary  $\mathbf{q}$  to seek the lowest eigenvalue among all  $\mathbf{q}$ ). The leading divergence can be easily identified by comparing all  $\Gamma_{min}^{ch}$  as  $\Lambda$  is reduced. The eigenvector of the most divergent  $\Gamma_{min}^{ch}$  reveals the orbital symmetry of the incipient order.

Fig. 3 shows the competition of the BCS, CDW, and Pomeranchuk channel for interaction strength  $g = 4$  and interaction range  $k_F R = 2$ . We observe from the upper panel that long before  $\Lambda_{IR}$  is reached, the BCS channel (in blue) develops into the leading divergence, with the other two channels trailing behind. The polar plot in the lower panel shows the eigenvector for  $\Gamma_{min}^{\text{BCS}}$  as a function of  $\phi$  as it varies from 0 to  $2\pi$  around the Fermi surface. It features 6 nodes, and can be fit nicely by  $f_{\text{BCS}}(\phi) = A \cos(3\phi - \phi_0)$ . The evidence unambiguously points to an  $\ell = 3$ , or  $f$ -wave, superfluid phase. Another example is shown in Fig. 4 for  $g = 6$  and  $k_F R = 5$ . While the flow looks rather similar to Fig. 2 and the leading instability remains in the BCS channel (upper panel), the eigenvector (lower panel) tells a different story. The orbital symmetry in this case is clearly different, suggesting an  $\ell = 5$ , or  $h$ -wave superfluid instead. Yet another example is shown in Fig. 5. Here none of the channel matrix eigenvalues develops divergence as  $\Lambda_{IR}$  is reached.

Similar FRG analysis can be performed for other parameter values on the  $(g, R)$  plane, and the results are summarized in the phase diagram shown in Fig. 1. The most striking feature of the phase diagram is a series of superfluid phases with Cooper pair angular momentum  $\ell = 3, 5, 7, 9$ . The empty circles mark the phase boundary, and the background false color shows the critical scale  $\Lambda_c$  serving as a rough estimate of the  $T_c$  of each ordered phase. The overall shape of the phase diagram resembles a hand with the index, middle, ring, and little finger. Note that  $p$ -wave superfluid with  $\ell = 1$ , or the ‘‘thumb,’’ is missing.

The phase boundaries (empty circles) in Fig. 1 are determined numerically as follows. In the first method, we decompose the eigenvector  $f_{\text{BCS}}(\phi)$  corresponding to  $\Gamma_{min}^{\text{BCS}}$  in the basis  $\{\cos(\ell\phi)\}$  with odd  $\ell \geq 1$ . We find



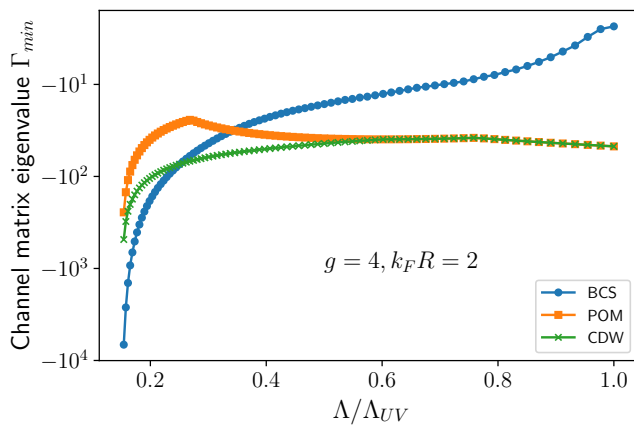


FIG. 3. The FRG flow for parameter  $g = 4$  and  $k_F R = 2$ . Upper panel: the most negative eigenvalue,  $\Gamma_{min}$ , in the BCS, Pomeranchuk, and CDW channel. As the sliding RG scale  $\Lambda$  is reduced from  $\Lambda_{UV}$ , BCS becomes the leading instability. Lower panel: the eigenvector  $f_{BCS}(\phi)$  corresponding to the BCS instability, with  $\phi$  going from  $0^\circ$  to  $360^\circ$  around the Fermi surface. Its nodal structure shows  $f$ -wave pairing with angular momentum  $\ell = 3$  (see main text).

that there is only one dominant  $\ell$  component in each superfluid phase, and the value of  $\ell$  jumps at the phase boundaries to form a terrace as  $k_F R$  is varied along a vertical cut at constant  $g = 9$  (in blue, Fig. 6). In the next method, we plot the second most negative eigenvalue of  $V_{BCS}$  (in magenta, Fig. 6). The idea is that as a phase boundary is approached, say going from the  $f$ -wave to the  $h$ -wave phase, the lowest two eigenvalues of  $V_{BCS}$  are expected to become degenerate. Thus, the second lowest eigenvalue will take a dip whenever a phase boundary is crossed. Fig. 6 shows that the phase boundaries determined from these two independent measures agree well with each other. And there is no indication of phase coexistence.

We stress that the empty circles in Fig. 1 represent only part of the phase boundaries. For small  $g$  or large  $R$ , the critical scale  $\Lambda_c$  is pushed down toward  $\Lambda_{IR}$ , making it challenging to reliably determine the phase bound-

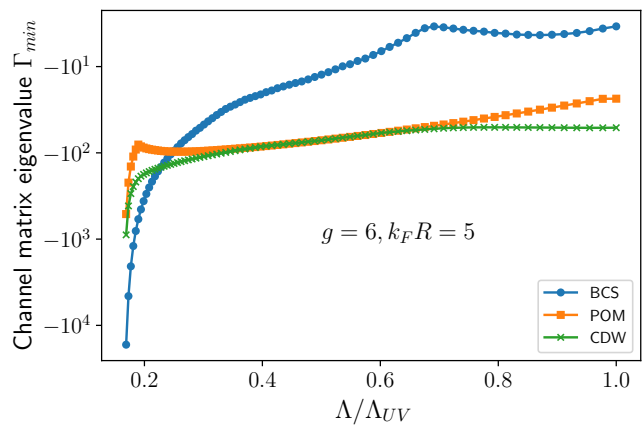


FIG. 4. Evidence of  $h$ -wave pairing from FRG for parameter  $g = 6$  and  $k_F R = 5$ . Upper panel: the competition between the BCS, Pomeranchuk, and CDW instability. Lower panel: the eigenvector  $f_{BCS}(\phi)$  can be fit by  $A \cos(5\phi - \phi_0)$ , pointing clearly to  $h$ -wave pairing with  $\ell = 5$ .

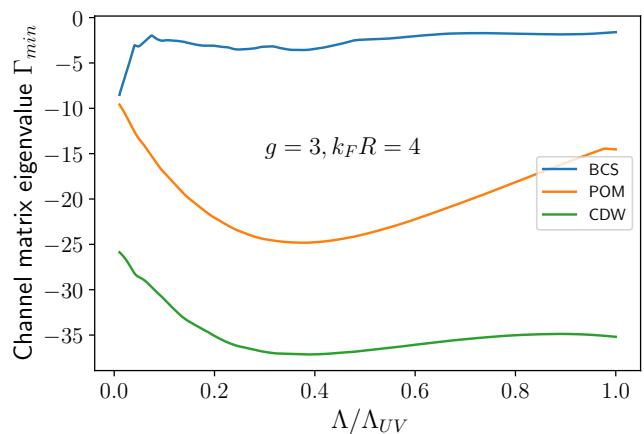


FIG. 5. Absence of long-range order for parameter  $g = 3$  and  $k_F R = 4$ . In contrast to Fig. 3 and Fig. 4, no divergence is visible as  $\Lambda$  is reduced down to  $\Lambda_{IR}$ .

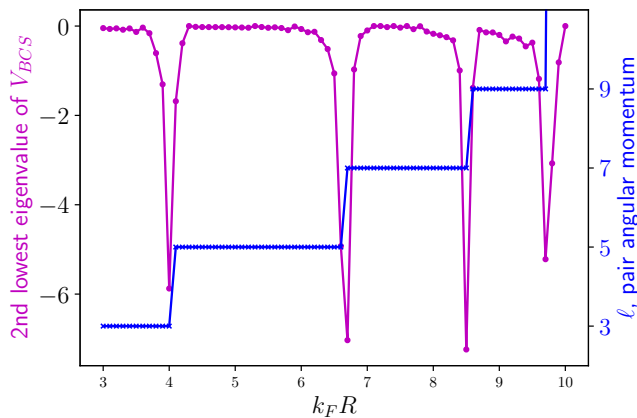


FIG. 6. Detecting the phase transitions along the vertical cut  $g = 9$  using two independent measures: (a) the pair angular momentum  $\ell$  extracted from  $f_{\text{BCS}}(\phi)$ , in color blue; and (b) the second lowest eigenvalue of the BCS channel matrix  $V_{\text{BCS}}$  (rescaled by  $10^3$ ), in color magenta. The phase boundaries from the two methods agree with each other.

ary using the methods outlined above. For this reason, only well resolved data points are presented. For example, both the  $f$ - and  $h$ -wave superfluid persist to lower  $g$  values with significantly reduced  $T_c$ , and their phase boundaries are expected to extend to the left as well. Superfluid phases with  $\ell > 9$  may exist at larger  $g$  and  $R$  values (not shown in Fig. 1), they are not well resolved due to the limitation of our angular grid and the diminishing  $T_c$  values.

Despite the apparent simplicity of our model, the phase diagram in Fig. 1 is quite rich and to our knowledge has not been reported before. Let us recall that generalizing the Kohn-Luttinger analysis to spin-1/2 Fermi gas with short-range repulsion in 2D predicts a  $p$ -wave superfluid state [19], which has gone missing in our case. It is also worthwhile to compare Fig. 1 to the phase diagram of the Rydberg-dressed Fermi gas in 2D, which harbors an  $f$ -wave superfluid that becomes intertwined with, and eventually yields to a CDW as the interaction range is increased [21]. Here, we do not see a CDW phase, because it is pushed to very high  $g$  values,  $g > 15$ , according to the random phase approximation. Instead, we see the emergence of a series of superfluid phases with higher angular momentum pairing.

Since the FRG calculation involves delicate interplays of particle-particle and particle-hole fluctuations on a sliding momentum/energy scale, one might wish a simpler “explanation” of how the bare repulsion is turned into a pairing glue. In the next section, we shed more light on these phases using perturbation theory.

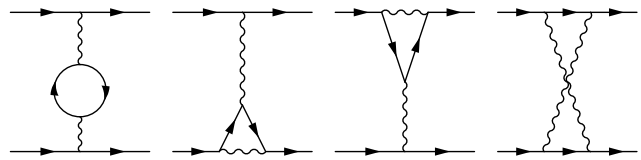


FIG. 7. The four Kohn-Luttinger diagrams as the second order contributions to the effective interaction. From left to right are  $D_1$ ,  $D_2$ ,  $D_3$  and  $D_4$ .

#### IV. INSIGHTS FROM PERTURBATION THEORY

The superfluid phases occupy a large portion of the parameter space in Fig. 1. A perturbation expansion in power series of  $V_0$  will not be justified everywhere, e.g. when  $V_0$  or  $g$  is large. However, it is well recognized that in the dilute, low-density limit (corresponding to small  $k_F R$ ), a perturbative expansion is possible even for large  $g$  [29]. With these caveats in mind, our main objective in this section is to look for the trends (rather than the exact numbers) suggested by perturbation theory.

To the first order of  $V_0$ , the effective interaction is given by the bare repulsion in Eq. (4). As shown in Fig. 2, all its angular components  $\Gamma_\ell^{(1)}$  are positive. For  $k_F R \leq 2$ ,  $\Gamma_{\ell=1}^{(1)}$  dominates, with all other components negligibly small. To order  $V_0^2$ , the corrections to the effective interaction in the Cooper channel consist of four contributions shown in Fig. 7, often referred to as the Kohn-Luttinger diagrams [15]. They are vertex functions describing a fermion pair  $(\mathbf{p}, -\mathbf{p})$  being scattered to  $(\mathbf{p}', -\mathbf{p}')$  that involves two bare interactions (wavy lines) and two internal fermion propagators (solid lines). The first diagram contains a particle-hole bubble,

$$D_1 = -i \int \frac{d^2 \mathbf{k} d\omega}{(2\pi)^3} v(\mathbf{q})v(\mathbf{q})G_0(k)G_0(k+q).$$

Here for spin-polarized fermions, the factor 2 associated with the fermion bubble is absent but the negative sign is retained.  $G_0$  is the bare fermion Green function at  $T = 0$  (different from the scale-dependent Green function in the previous section), the 4-momentum  $k = (\omega, \mathbf{k})$ , and similarly  $q = (\Omega, \mathbf{q})$  with the momentum transfer  $\mathbf{q} = \mathbf{p}' - \mathbf{p}$ . The second diagram contains the vertex correction

$$D_2 = i \int \frac{d^2 \mathbf{k} d\omega}{(2\pi)^3} v(\mathbf{q})v(-\mathbf{p} - \mathbf{k})G_0(k)G_0(k+q).$$

The third diagram is very similar to the second,

$$D_3 = i \int \frac{d^2 \mathbf{k} d\omega}{(2\pi)^3} v(\mathbf{q})v(\mathbf{p}' - \mathbf{k})G_0(k)G_0(k+q).$$

And the fourth diagram is the exchange scattering

$$D_4 = i \int \frac{d^2 \mathbf{k} d\omega}{(2\pi)^3} v(\mathbf{p} - \mathbf{k})v(\mathbf{p}' - \mathbf{k})G_0(k)G_0(k - p - p').$$

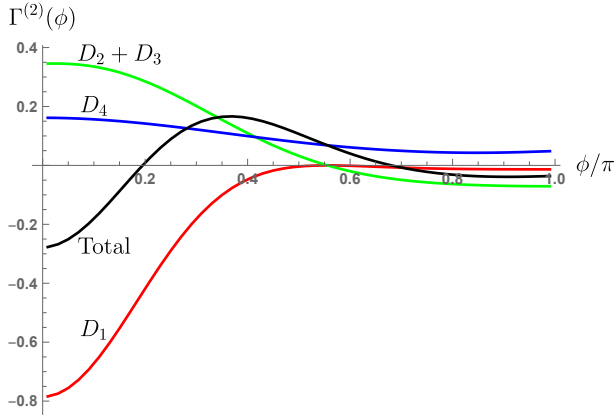


FIG. 8. The second order contribution to the effective interaction,  $\Gamma^{(2)}(\phi)$ . It is defined in Eq. (12) and contains the contributions from four Kohn-Luttinger diagrams,  $D_1$  to  $D_4$ . Most noticeably,  $D_1$  turns negative (attractive). The black curve is the total sum of all four diagrams.  $k_F R = 2.5$ .

To evaluate these diagrams, first the  $\omega$  integral is carried out analytically, then the integration over  $\mathbf{k}$  is computed numerically.

The second-order contribution to the effective interaction is given by summing over  $D_1$  to  $D_4$  for  $\mathbf{p}$  and  $\mathbf{p}'$  on the Fermi surface. In unit of  $(2\pi V_0 R^2)$ , the result can be organized into

$$\Gamma^{(2)}(\phi) = \frac{\pi}{g} \sum_{i=1}^4 D_i. \quad (12)$$

As an example, the function  $\Gamma^{(2)}(\phi)$  for the case of  $Rk_F = 2.5$  is plotted in Fig. 8. We find that the contribution for diagram  $D_1$  (the red curve) turns negative for a significant range of  $\phi$  values, e.g.  $\phi < \pi$ , while in the same region the contributions from  $D_2 + D_3$  (in green) and  $D_4$  (in blue) remain positive. As a result, the total sum (the black curve) develops oscillations with  $\phi$ . This clearly shows that density fluctuations as captured by  $D_1$  plays an important role in making the pairing glue. We can further decompose  $\Gamma^{(2)}(\phi)$  into angular momentum channels, the resulting  $\Gamma_\ell^{(2)}$  for  $\ell = 1$  (blue square),  $\ell = 3$  (orange circle),  $\ell = 5$  (green triangle), and  $\ell = 7$  (red plus) are shown in Fig. 9. One observes that as  $R$  is increased, all components eventually turn attractive. For  $\ell = 3$ , the effect is most pronounced around  $R \sim 3.7/k_F$ .

Now we can combine the second-order contribution  $\Gamma_\ell^{(2)}$  with the bare repulsion  $\Gamma_\ell^{(1)}$ . We ask at what critical values  $g = g_c$  the total effective interaction turns attractive, i.e.,

$$\Gamma_\ell^{(0)} + \frac{g_c}{\pi} \Gamma_\ell^{(2)} = 0. \quad (13)$$

Solving this equation for  $g_c$ , we arrive at the perturbative phase diagram in Fig. 10, where the phase boundaries of the  $\ell = 1, 3, 5, 7$  superfluid are plotted using the same symbols as in Fig. 9. The unconventional Cooper

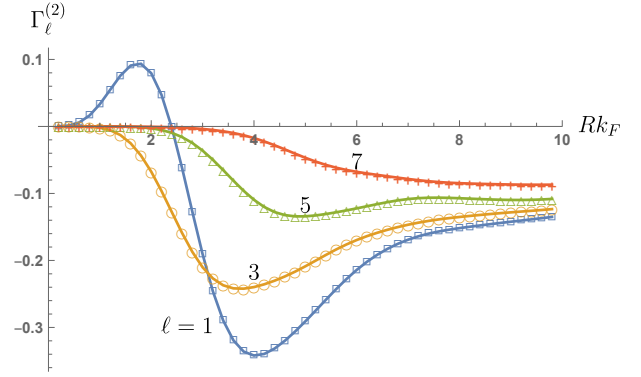


FIG. 9. The second order contribution to pairing interaction  $\Gamma_\ell^{(2)}$  in angular momentum channel  $\ell = 1, 3, 5$ , and  $7$ . They all become attractive for sufficiently large  $k_F R$ .

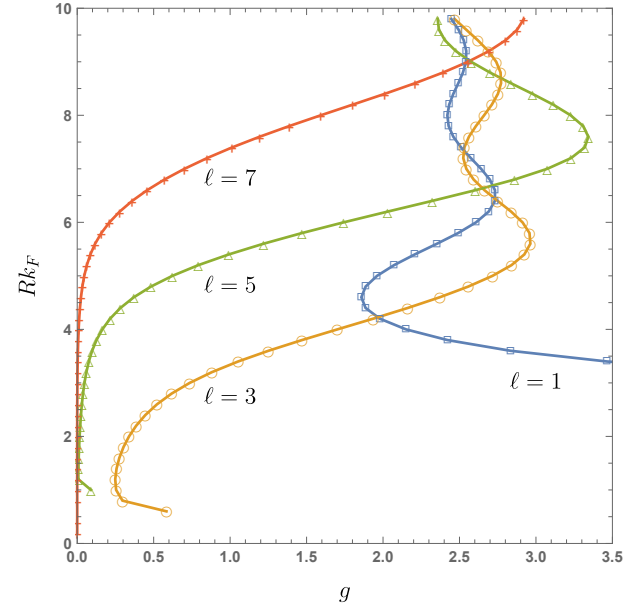


FIG. 10. The onset of superfluid phases with  $\ell = 1$  (blue),  $3$  (orange),  $5$  (green), and  $7$  (red) according to second order perturbation theory. The data points represent the critical value  $g_c$ . For fixed  $k_F R$ , pairing occurs for  $g > g_c$ .

pairing discovered here is to some degree parallel to the high partial-wave pairing in the particle-hole (or density wave) channel predicted for fermionic systems with soft-core interactions [30]. One crucial difference is that the high partial-wave pairing in the particle-particle (superfluid) channel only requires time-reversal or parity symmetries of the Fermi surface whereas the corresponding particle-hole pairing requires Fermi surface nesting effects in addition [30].

Now we are in position to compare Fig. 10 to Fig. 1. According to the second order perturbation theory,  $p$ -wave pairing (blue square in Fig. 10) is pushed toward large  $g$  and  $R$  values. This is mainly because the bare interaction  $\Gamma_{\ell=1}^{(1)}$  is large and positive, and therefore rather

hard to overcome. Another reason is that  $\Gamma_{\ell=1}^{(2)}$  only becomes negative when  $R > 2.4$  as shown in Fig. 9. Note that according to FRG which contains many more diagrams to higher order,  $p$ -wave pairing is actually absent from the phase diagram. The onset of  $f$ -wave pairing (orange circles) in Fig. 10 is roughly consistent with the FRG phase boundary except for large  $R$ . It is stabilized within the window between  $k_F R \sim 2$  and  $k_F R \sim 4$ , where the bare repulsion  $\Gamma_{\ell=3}^{(1)}$  is not particularly strong but  $\Gamma_{\ell=3}^{(2)}$  already turns negative. For these reasons, the onset of  $f$ -wave superfluid requires much a smaller  $g_c$  than the  $p$ -wave. In short, perturbation theory correctly predicts that  $f$ -wave superfluid is preferred over  $p$ -wave in our model. Pairing with larger  $\ell$  moves successively to larger  $R$  and lower  $g_c$ , and the relative positions of the  $\ell = 3, 5, 7$  lobes from Fig. 10 are roughly in line with Fig. 1.

In summary, it is fair to say that the perturbative calculation above captures some of the rough features of the FRG phase diagram. On the one hand, it is able to pinpoint certain microscopic processes (e.g.  $D_1$  to  $D_4$ ) that work together to turn the effective interaction attractive, i.e. to provide the pairing glue. On the other hand, the details of Fig. 10 differ significantly from Fig. 1. This is not surprising, for the perturbation results are not reliable at higher  $k_F R$  values.

## V. SUMMARY AND OUTLOOK

We have presented evidence for superfluid phases with Cooper pair angular momentum  $\ell = 3, 5, 7, 9$  in a model system of spin-polarized fermions with short-range repulsive interactions. Our main goal is to elucidate how the repulsion is turned into glue that binds the fermions into Cooper pairs. While FRG provides the full picture and more accurate results, some of the trends and gross features can already be appreciated from perturbative considerations. According to our calculation, it is inaccurate to only credit density fluctuations such as diagram  $D_1$  for providing the glue, because other processes also contribute to the renormalization of the effective interaction, e.g. to the second order correction  $\Gamma_{\ell}^{(2)}$ . Comparing the phase diagram Fig. 1 with the case of Rydberg-dressed Fermi gas [21] clearly shows that *the form of the bare interaction matters*.

These considerations naturally lead to the open question: assuming that we can engineer arbitrary  $v(r)$  using the tricks of Atomic Molecular and Optical physics, which kind of bare repulsive interaction  $v(r)$  offers the best route toward superfluid with a reasonably high  $T_c$ ?

A heuristic argument is that we would like  $v(r)$  to have sharp features, so that its Fourier transform  $v(q)$  will acquire negative segments which could be potentially advantageous to pairing. While this intuition serves us well by inspiring the choice of Eq. (1) in the present work, it must be kept in mind that this is not a first order effect. For example, in our example, to the first order of  $V_0$ , all  $\Gamma_{\ell}^{(1)} > 0$ ; one must carefully compute the effective interaction by taking many-body processes into account. Roughly speaking, higher angular momentum (rather than  $p$ -wave) pairing is preferred because there is less bare repulsion to overcome, and it can take better advantage of the oscillation of  $\Gamma^{(2)}(\phi)$  around the Fermi surface. It may be challenging to realize the simple model and the phases predicted here in near future experiments. But the lessons learned from the case study, including the general trend and the underlying mechanism, can benefit the ongoing effort to engineer stronger pair glue in repulsive Fermi gases.

Previously  $f$ -wave pairing has been discussed for example in the context of superfluid helium three [31, 32] as well as cold atoms on optical lattice [33], but in those cases it is stabilized by very different mechanisms. We stress that in the present work, the bare interaction is repulsive and the system is two dimensional. This differs from previous studies on Rydberg-dressed Fermi gas in 3D with attractive interactions [34] including the appearance of high partial wave pairing [35] by coupling to a  $nD$  state. In our case, pairing beyond  $f$ -wave (with  $\ell \geq 5$ ) requires larger value of  $k_F R$ , i.e. away from the dilute limit. It remains an open problem regarding what happens if we generalize the model to spin-1/2 Fermi gases, where the effect of long-range potentials on pairing has been discussed [36, 37]. Whether the  $f$ -wave pairing found here can lead to topological superfluid state is another question left for future study.

## ACKNOWLEDGMENTS

This work is supported by NSF grant PHY-206419 and AFOSR grant FA9550-23-1-0598 (EZ), TUBITAK 2236 Co-funded Brain Circulation Scheme 2 (CoCirculation2) Project No. 120C066 (AK), National Program on Key Basic Research Project of China Grant 2021YFA1400900 (XL), and National Natural Science Foundation of China Grant 11934002 (XL). EZ acknowledges illuminating discussions with A. Chubukov, and he is indebted to J. A. Sauls for questions that led to the comparison between  $p$ - and  $f$ -wave pairing in Section IV. Part of this work (EZ) is performed at Aspen Center for Physics, which is supported by NSF grant PHY-2210452.

[1] C. A. Regal, C. Ticknor, J. L. Bohn, and D. S. Jin, Tuning  $p$ -wave interactions in an ultracold fermi gas of atoms,

Phys. Rev. Lett. **90**, 053201 (2003).

[2] J. Zhang, E. G. M. van Kempen, T. Bourdel,



- L. Khaykovich, J. Cubizolles, F. Chevy, M. Teichmann, L. Tarruell, S. J. J. M. F. Kokkelmans, and C. Salomon,  $p$ -wave feshbach resonances of ultracold  $^6\text{Li}$ , *Phys. Rev. A* **70**, 030702 (2004).
- [3] K. Günter, T. Stöferle, H. Moritz, M. Köhl, and T. Esslinger,  $p$ -wave interactions in low-dimensional fermionic gases, *Phys. Rev. Lett.* **95**, 230401 (2005).
- [4] M. Waseem, T. Saito, J. Yoshida, and T. Mukaiyama, Two-body relaxation in a fermi gas at a  $p$ -wave feshbach resonance, *Phys. Rev. A* **96**, 062704 (2017).
- [5] Y.-T. Chang, R. Senaratne, D. Cavazos-Cavazos, and R. G. Hulet, Collisional loss of one-dimensional fermions near a  $p$ -wave feshbach resonance, *Phys. Rev. Lett.* **125**, 263402 (2020).
- [6] A. S. Marcum, F. R. Fonta, A. M. Ismail, and K. M. O'Hara, Suppression of three-body loss near a  $p$ -wave resonance due to quasi-1D confinement, [arXiv:2007.15783](https://arxiv.org/abs/2007.15783) (2020).
- [7] C. Luciuk, S. Trotzky, S. Smale, Z. Yu, S. Zhang, and J. H. Thywissen, Evidence for universal relations describing a gas with  $p$ -wave interactions, *Nature Physics* **12**, 599 (2016).
- [8] V. Venu, P. Xu, M. Mamaev, F. Corapi, T. Bilitewski, J. P. D'Incao, C. J. Fujiwara, A. M. Rey, and J. H. Thywissen, Unitary  $p$ -wave interactions between fermions in an optical lattice, *Nature* **613**, 262 (2023).
- [9] P. W. Anderson, Is there glue in cuprate superconductors?, *Science* **316**, 1705 (2007).
- [10] P. Monthoux, D. Pines, and G. Lonzarich, Superconductivity without phonons, *Nature* **450**, 1177 (2007).
- [11] P.-G. De Gennes, *Superconductivity of metals and alloys* (CRC press, 2018).
- [12] S. Maiti and A. V. Chubukov, Superconductivity from repulsive interaction, in *AIP Conference Proceedings*, Vol. 1550 (American Institute of Physics, 2013) pp. 3–73.
- [13] M. Y. Kagan, V. A. Mitskan, and M. M. Korovushkin, Anomalous superconductivity and superfluidity in repulsive fermion systems, *Physics-Uspekhi* **58**, 733 (2015).
- [14] R. Shankar, Renormalization-group approach to interacting fermions, *Rev. Mod. Phys.* **66**, 129 (1994).
- [15] W. Kohn and J. M. Luttinger, New Mechanism for Superconductivity, *Phys. Rev. Lett.* **15**, 524 (1965).
- [16] J. M. Luttinger, New mechanism for superconductivity, *Phys. Rev.* **150**, 202 (1966).
- [17] D. Fay and A. Layzer, Superfluidity of low-density fermion systems, *Phys. Rev. Lett.* **20**, 187 (1968).
- [18] M. Y. Kagan and A. Chubukov, Possibility of a superfluid transition in a slightly nonideal fermi gas with repulsion, *JETP Lett* **47**, 614 (1988).
- [19] A. V. Chubukov, Kohn-Luttinger effect and the instability of a two-dimensional repulsive Fermi liquid at  $T=0$ , *Phys. Rev. B* **48**, 1097 (1993).
- [20] E. Guardado-Sanchez, B. M. Spar, P. Schauss, R. Belyansky, J. T. Young, P. Bienias, A. V. Gorshkov, T. Iadecola, and W. S. Bakr, Quench dynamics of a fermi gas with strong nonlocal interactions, *Phys. Rev. X* **11**, 021036 (2021).
- [21] A. Keleş, E. Zhao, and X. Li,  $f$ -wave superfluidity from repulsive interaction in rydberg-dressed fermi gas, *Phys. Rev. A* **101**, 023624 (2020).
- [22] W. Metzner, M. Salmhofer, C. Honerkamp, V. Meden, and K. Schönhammer, Functional renormalization group approach to correlated fermion systems, *Rev. Mod. Phys.* **84**, 299 (2012).
- [23] P. Kopietz, L. Bartosch, and F. Schutz, *Introduction to the Functional Renormalization Group (Lecture Notes in Physics)* (Springer, 2010).
- [24] A. Keleş and E. Zhao, Competing many-body instabilities in two-dimensional dipolar fermi gases, *Phys. Rev. A* **94**, 033616 (2016).
- [25] S. G. Bhongale, L. Mathey, S.-W. Tsai, C. W. Clark, and E. Zhao, Bond order solid of two-dimensional dipolar fermions, *Phys. Rev. Lett.* **108**, 145301 (2012).
- [26] S. G. Bhongale, L. Mathey, S.-W. Tsai, C. W. Clark, and E. Zhao, Unconventional spin-density waves in dipolar fermi gases, *Phys. Rev. A* **87**, 043604 (2013).
- [27] S. G. Bhongale, L. Mathey, E. Zhao, S. F. Yelin, and M. Lemeshko, Quantum Phases of Quadrupolar Fermi Gases in Optical Lattices, *Phys. Rev. Lett.* **110**, 155301 (2013).
- [28] R. Shankar, Renormalization-group approach to interacting fermions, *Rev. Mod. Phys.* **66**, 129 (1994).
- [29] M. Baranov, A. Chubukov, and M. Yu. Kagan, Superconductivity and superfluidity in fermi systems with repulsive interactions, *International Journal of Modern Physics B* **6**, 2471 (1992).
- [30] X. Li and S. D. Sarma, *Exotic topological density waves in cold atomic Rydberg-dressed fermions*, *Nat. Commun.* **6**, 7137 (2015).
- [31] J. A. Sauls,  $f$ -wave correlations in superfluid  $^3\text{He}$ , *Phys. Rev. B* **34**, 4861 (1986).
- [32] J. P. Davis, H. Choi, J. Pollanen, and W. P. Halperin, Collective modes and  $f$ -wave pairing interactions in superfluid  $^3\text{He}$ , *Phys. Rev. Lett.* **97**, 115301 (2006).
- [33] W.-C. Lee, C. Wu, and S. Das Sarma,  $f$ -wave pairing of cold atoms in optical lattices, *Phys. Rev. A* **82**, 053611 (2010).
- [34] B. Xiong, H. H. Jen, and D.-W. Wang, Topological superfluid by blockade effects in a rydberg-dressed fermi gas, *Phys. Rev. A* **90**, 013631 (2014).
- [35] Y. Zhou, R. Nath, H. Wu, I. Lesanovsky, and W. Li, Multipolar fermi-surface deformation in a rydberg-dressed fermi gas with long-range anisotropic interactions, *Phys. Rev. A* **104**, L061302 (2021).
- [36] A. S. Alexandrov and V. V. Kabanov, Unconventional high-temperature superconductivity from repulsive interactions: Theoretical constraints, *Phys. Rev. Lett.* **106**, 136403 (2011).
- [37] S. Raghu, E. Berg, A. V. Chubukov, and S. A. Kivelson, Effects of longer-range interactions on unconventional superconductivity, *Phys. Rev. B* **85**, 024516 (2012).